Engineering Structures 41 (2012) 320–334

Contents lists available at SciVerse ScienceDirect

Engineering Structures

journal homepage: www.elsevier.com/locate/engstruct

# Structural behavior and modeling of full-scale composite structural insulated wall panels

Mohammed A. Mousa [a,b], Nasim Uddin [a,*]

[a] Department of Civil, Construction and Environmental Engineering, University of Alabama at Birmingham, Birmingham, AL 35294-4440, United States
[b] Department of Civil Engineering, Faculty of Engineering at Shoubra, Benha University, Cairo, Egypt

ARTICLE INFO

*Article history:*
Received 27 April 2010
Revised 12 March 2012
Accepted 12 March 2012

*Keywords:*
Sandwich structures
Thermoplastic composites
Wall testing

ABSTRACT

This paper investigates the structural behavior of a new type of Composite Structural Insulated Panels (CSIPs) for load-bearing wall applications. The proposed composite panel is made of low cost orthotropic thermoplastic glass/polypropylene (glass-PP) laminate as a facesheet and Expanded Polystyrene Foam (EPS) as a core. The proposed CSIP wall is intended to overcome problems of the traditional Structural Insulated Panels (SIPs). These problems include termite attack, disintegration due to flood water, mold buildups and poor penetration resistance against wind borne debris. Full scale experimental testing for three CSIP panels was conducted to study the behavior of CSIP walls under eccentric load. Further, pull off strength tests were conducted to determine the bonding strength between the glass-PP facesheet and EPS foam core. Facesheet/core debonding was observed to be the general mode of failure. This study provides also analytical models to predict the interfacial tensile stress at the core/facesheet interface, critical wrinkling stress and deflections for a structural CSIP wall member. In addition, finite element modeling was also conducted using ANSYS software in order to model the response of CSIPs walls under in-plane loading. Experimental results were validated using the proposed analytical models and FE modeling, and were observed to be in good agreement. Furthermore, a parametric FE study was conducted to investigate the influence of key design parameters on the behavior of CSIPs. The study showed that span-to-depth ratio and core density have a significant effect on the structural performance of CSIP wall panels.


## 1. Introduction

Traditional Structural Insulated Panels (SIPs) are made of wood-based facing and foam core. These SIPs are often subjected to termite attack, mold buildups, rotting and have poor penetration resistance against wind borne debris. So the need for an effective alternative became an urgency. Composites are a great candidate to replace the traditional panels for housing applications. This paper presents a new composite panel system: Composite Structural Insulated Panels (CSIPs) which were developed by the authors. CSIPs are made of low cost orthotropic thermoplastic glass/polypropylene (glass-PP) laminate as facesheets and Expanded Polystyrene Foam (EPS) as a core. CSIPs take the concept of the sandwich construction that consists of two strong, thin facings and a soft lightweight thicker core. The facesheets carry the bending stresses while the thick core resists the shear loads and stabilizes the faces against bulking or wrinkling [1]. The core also increases the stiffness of the structure by holding the facesheets apart. Core materials normally have lower mechanical properties compared to those of facesheets. Despite the high strength resulting from this combination, deflection and debonding are other significant aspects that are considered in the design of CSIPs [2]. Several investigations have been conducted at the University of Alabama at Birmingham (UAB) by the authors and others on developing composite panels for building applications using rigid and soft cores with thermoset and thermoplastic facesheets [2–8]. It was demonstrated by these studies that the developed panels can provide much higher strength, stiffness, and creep resistance than traditional ones that are made with wood-based facing. The developed CSIPs have a very high facesheet/core moduli ratio ($E_f/E_c$ = 12,500) compared with the ordinary sandwich construction where the ratio is normally limited to 1000 [1]. Further, CSIPs are characterized by low cost, high strength to weight ratio, and lower skill required for field construction, etc. These panels can be used for different elements in the structure, including structural elements (e.g., load bearing walls, floors, and roofs) and non-structural elements (e.g., non-load bearing walls, lintels, and partitions).

Many theoretical and experimental studies have been conducted on sandwich construction to investigate their behavior under different types of loadings including in-plane and out-of-plane loadings. A general review of failure modes of composite sandwich beams

* Corresponding author.
*E-mail addresses:* mmousa@uab.edu (M.A. Mousa), nuddin@uab.edu (N. Uddin).

0141-0296/$ - see front matter © 2012 Elsevier Ltd. All rights reserved.
http://dx.doi.org/10.1016/j.engstruct.2012.03.028

construction was given by Daniel et al. [9] while those of sandwich wall were given by Gdoutos et al. [10]. Failures modes for sandwich beams include yielding of facesheet in tension, core shear failure, and local buckling of facesheet in compression which is known as wrinkling of facesheets. Failure modes of sandwich wall include global buckling, local buckling "wrinkling", and core failure. In case of global buckling, the core may exhibit a substantial shearing deformation whereas in case of local buckling the core acts as an elastic foundation for the facesheets in compression [11,12]. The local buckling can be outward or downward. Outward buckling is known as debonding whereas downward buckling is known as core crushing. The former occurs in case of a sandwich panel with closed cell cores (e.g., EPS foam) while the latter is more characteristic of sandwich panels with open cell cores (e.g., honeycomb core) [13]. Among the first to study the behavior of sandwich panels were Gough et al. [14] and Hoff and Mautner [15]. They tested sandwich specimens under compressive loading and observed that the general mode of failure was facesheet wrinkling. They also developed formulas to predict the stress in the facesheet at wrinkling. These formulas were then modified to fit the experimental results. The results showed that the wrinkling stress is independent of loading and boundary condition and mainly depends on the facesheets and core moduli. The objectives of the current work are: to investigate the structural behavior of full scale CSIP walls under eccentric loading; to develop models to determine stresses associated with debonding, and to develop a model for equivalent CSIP wall stiffness considering the core deformation effects to determine the deflection of a CSIP wall member.

## 2. Materials and specimens

CSIP walls that are developed and evaluated in this study are made of low cost thermoplastic glass/polypropylene (glass-PP) laminate as a facesheet and Expanded Polystyrene Foam (EPS) as a core (Fig. 1). Thermoplastics (TP) polymers offer advantages in terms of short processing time, extended shelf life, and low-cost raw material. TP also possess the advantages of high toughness, superior impact property, and ease of reshaping and recycling over thermoset polymer composites.

Thermoplastic laminates used in this study consist of 70% bi-directional E-glass fibers impregnated with poly-propylene (PP) resin. Thermoplastic composites are produced using a hot-melt impregnation process, also called a DRIFT process [16]. In this research, the 3.04 mm (0.12 in.) thick glass-PP composite sheets were directly obtained from the manufacturer [17]. The mechanical properties of glass-PP composites used in this research are listed in Table 1.

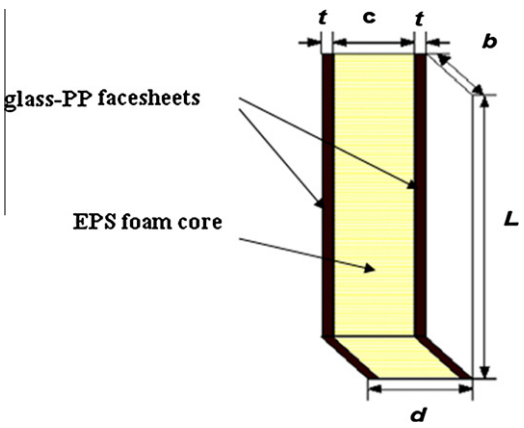


**Fig. 1.** Schematic diagram for the proposed CSIPs wall.

**Table 1**
Properties of the glass-PP facesheets.

| | |
|---|---|
| Nominal thickness, $t$ | 0.12 in. (3.04 mm) |
| Weight% of glass fiber | 70% |
| Density ($\rho_f$) | 61 PCF (980 kg/m$^3$) |
| Longitudinal modulus ($E_x$) | 2,200,000 psi (15, 169 MPa) |
| Transverse modulus ($E_y$) | 2,200,000 psi (15, 169 MPa) |
| Through thickness modulus ($E_z$) | 149, 350 psi (1030 MPa) |
| $\upsilon_{xy}$ | 0.11 |
| $\upsilon_{yz}$ | 0.22 |
| $\upsilon_{xz}$ | 0.22 |
| $G_{xy}$ | 261,000 psi (1800 MPa) |
| $G_{yz}$ | 108, 750 psi (750 MPa) |
| $G_{xz}$ | 108, 750 psi (750 MPa) |
| Tensile strength | 46,000 psi (317 MPa) |
| Flexural strength | 60,000 psi (414 MPa) |

**Table 2**
Properties of the EPS core.

| | |
|---|---|
| Nominal thickness, $c$ | 5.5 in. (140 mm) |
| Density ($\rho_c$) | 1 PCF (16 kg/m$^3$) |
| Elastic modulus ($E_c$) | 180–220 psi (1.2–1.5 MPa) |
| Flexural strength | 25–30 psi (0.1–0.2 MPa) |
| Shear modulus ($Gc$) | 280–320 psi (1.9–2.2 MPa) |
| Shear strength | 18–22 psi (0.1–0.15 MPa) |
| Tensile strength | 16–20 psi (0.11–0.14 MPa) |
| Compressive strength | 10–14 psi (0.07–0.1 MPa) |
| Poisson's ratio | 0.25 |

**Table 3**
Dimensions CSIP wall panels.

| | |
|---|---|
| Facesheet thickness ($t$) | 0.12 in. (3.04 mm) |
| Core thickness ($c$) | 5.5 in. (140 mm) |
| Total thickness ($d$) | 5.74 in. (146.08 mm) |
| Width ($b$) | 48 in. (1219.2 mm) |
| Length ($L$) | 96 in. (2438.4 mm) |

Foam is a material characterized by low cost and low weight. It also has good fire and thermal resistance as well as excellent impact properties. Because of these properties, it works very well as an insulation material. There are many types of foams, such as Polystyrene, Polyethylene, and Polyurethane foam. These types vary in both properties and cost. Because of the lower cost, Expanded Polystyrene Foam (EPS) was selected for use as a core for CSIPs. Table 2 describes the properties of the EPS foam used in this study as provided by the manufacturer [18]. All these properties lead finally to the high performance of the panels. The glass-PP facesheets were bonded to the EPS core using a hot-melt thermoplastic spray adhesive. This method of manufacturing is fast and less labor intensive than manufacturing of traditional SIPs. To ensure quality of processing, CSIPs wall panels tested in this study were manufactured at a casting and molding facility (Fig. 2). Facesheets and core thicknesses were optimized and designed according to a number of iterations using sandwich construction formulas. The overall dimensions (length and width) of the CSIP wall panels were maintained the same as that for traditional SIPs [19] which are given in Table 3.

### 2.1. Pull off strength testing

The adhesive used for bonding the facesheets to the core is the most important component in a sandwich structure. The use of proper adhesive ensures effective load transfer between facesheets and the core. It is well known that debonding between the core and

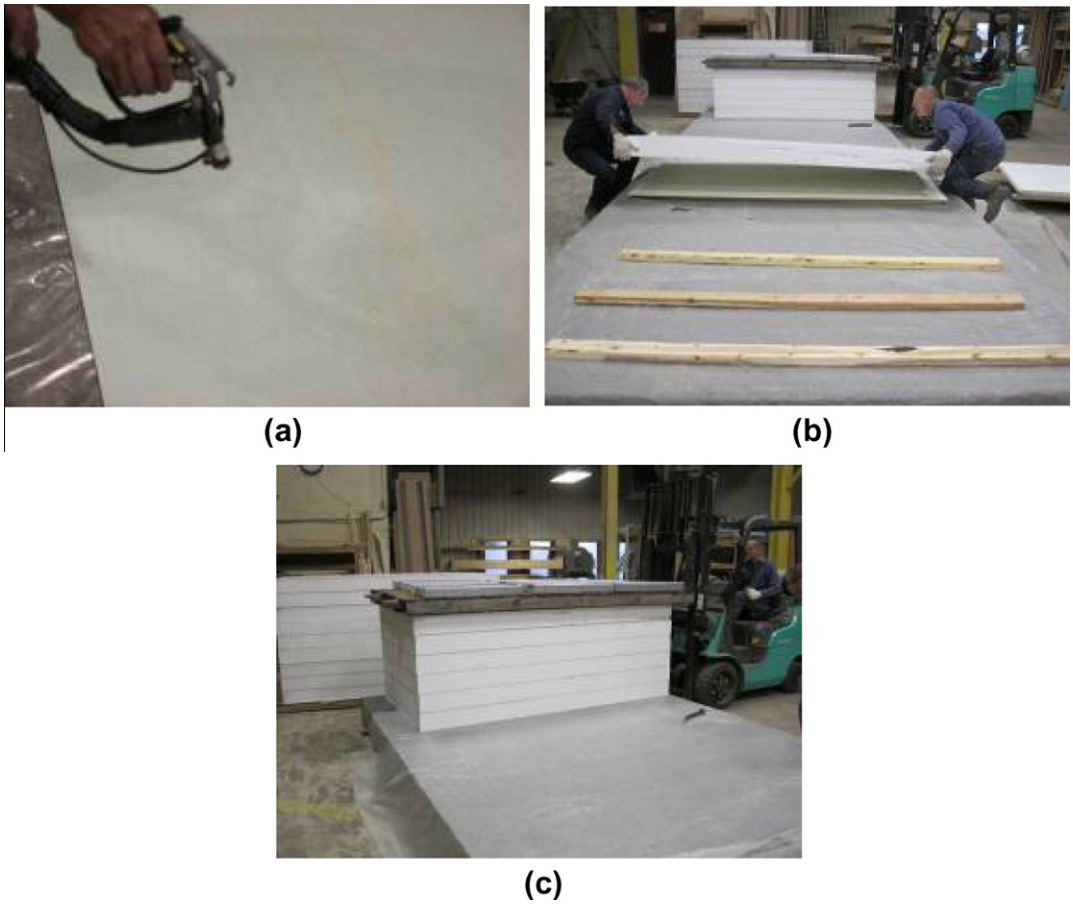


**Fig. 2.** Manufacturing of full scale CSIP walls: (a) spraying hot-melt adhesive on the facesheet, (b) placing foam core on the sprayed facesheet, and (c) ready panels stacked on to the floor.

the facesheet is the predominant mode of failure for sandwich composite structures, so choosing a proper adhesive is key in achieving the desired strength of the sandwich composite. As discussed above, spray adhesive was used to bond the glass-PP facesheets to EPS foam core. Normally, debonding occurs when the interfacial out of plane stresses exceeds the tensile strength of the core or that of the adhesive material. In order to determine the bond strength between the core and facesheets, pull off strength tests were conducted on CSIP specimens according to ASTM 1583-04 [20].

Three different adhesives were used in this test for bonding the facesheets to the core of the CSIPs in order to compare between them; hot-melt thermoplastic spray adhesive, the one that is used to fabricate the wall panel, thermoplastic film adhesive, and 3 M Fastbond™ water-based contact adhesive. Processing of specimens with spray adhesive was similar to that of wall panels. For specimens prepared using film adhesive, the facesheets were cleaned with the help of pressurized air to remove any loose dust. The facesheets were then cleaned with acetone to dissolve the sizing present on the laminates. Film adhesive was cut to the size of the facesheet and laid on top of the facesheet prior to placing them in the oven. The film adhesive melted in the temperature range of 65–74 °C (150–165 °F). After the adhesive was melted, the foam core was placed on top of the facesheet, ensuring proper alignment. The whole assembly was then flipped, and the bottom facesheet was adhered to the foam core in a similar manner. The sandwich was allowed to cool down in the oven for 15 min and was then taken out and stacked on the floor. For 3 M Fastbond, the adhesive is applied to the core substrate by means of a paintable brush then the facesheets are placed on top of core. The panels are then taken out and stacked on the floor.

Dyna Z-16 apparatus was used for checking the bond strength between the facesheet and the foam core. 50 mm diameter by 24 mm height aluminum test disks were bonded to the facesheet with 3 M scotch-weld epoxy adhesive as recommended in the Dyna-Z-16 operation manual [21]. According to ASTM 1583-04 [20], a core depth of 10 mm was chosen for the CSIPs. The Dyna-Z-16 apparatus is capable of applying a uni-axial tensile load on the test disks, which creates a concentrated stress beneath the test disks. A schematic for the Dyna-Z-16 apparatus is illustrated in

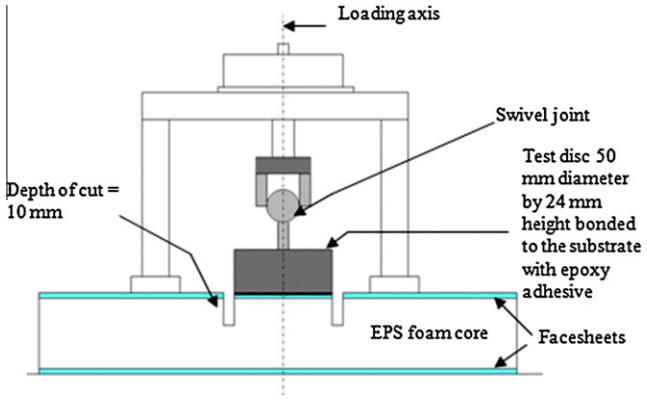


**Fig. 3.** Schematic of pull off strength testing (ASTM-C-1583-04).

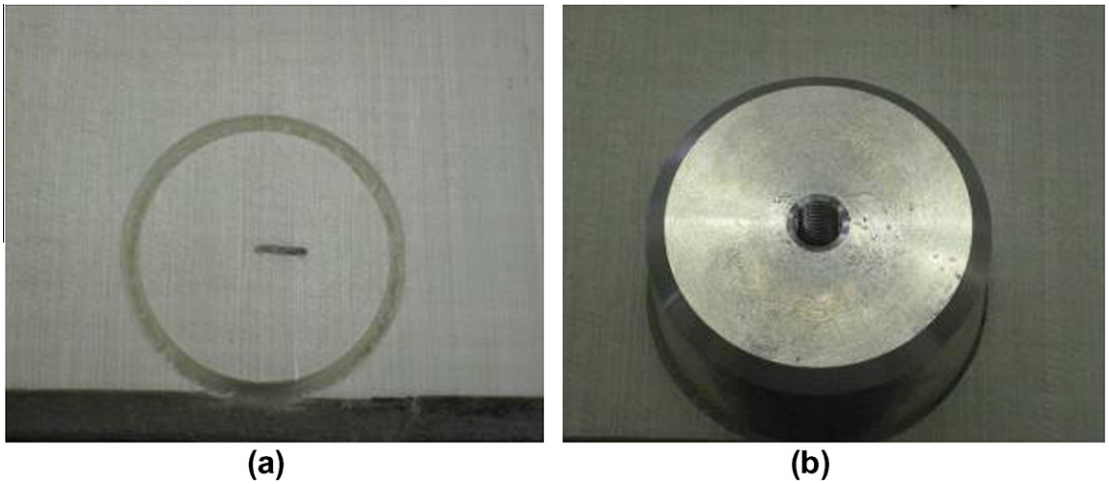


**Fig. 4.** Preparing the CSIP for pull off strength testing: (a) a cut of 10 mm is made, (b) an aluminum test disc is bonded to the facesheet with epoxy adhesive.

Fig. 3 while Fig. 4 shows the preparations of CSIP samples for pull off test. Three samples were tested for each type of adhesive.

The failure mode for spray and film specimens was in the form of a cohesive failure of the foam core (Fig. 5) which can be attributed to the fact that the applied uniaxial tensile stress is higher than that of the core material. On the other hand, for the 3 M Fastbond, the failure was in the form of adhesive failure between core and the facesheet. All and average results obtained from the pull-off test for two adhesives are plotted in Fig. 6. It can be seen from Fig. 6 that spray and film adhesives were comparable in terms of the bond strength which was about 0.17 MPa (24.6 psi) with standard deviation of 0.02 and 0.022; respectively. Comparing this strength with the core tensile strength (20 psi), demonstrates that the failure occurs because the out-of-plane stress just exceeded the tensile strength of core. For the 3 M Fastbond, the average bond strength was 0.063 MPa (9.14 psi) with standard deviation of 0.019. Although both spray and film adhesives provide similar results, spray adhesive is recommended for manufacturing the full-scale CSIPs due to its uniform wet-out and cost benefits compared with film adhesive.

## 3. Experimental procedure

### 3.1. Test-setup and loading

To characterize the structural response of CSIP wall panels, three CSIP wall panels were tested according to ASTM E-72 [22] which deals with testing structural panels for building applications. For most compression-loaded members, the line of action of the load does not act at the centroid due to dimension and construction errors. Accordingly, ASTM E-72 [22] recommends that these walls should be tested under eccentric compressive load by applying the load uniformly to the top cross section of the panels along a line parallel to the inside face at one-third the panels' thickness from inside which corresponds to an eccentricity of $d/6$ from the wall centroid. Deflection was measured using a 150 mm linear variable displacement transducer (LVDT). The structural behavior of the panel was analyzed by measuring surface strains on both faces of the panels. The schematic test-setup is shown in Fig. 7 while CSIP wall under loading is shown in Fig. 8. Since wall panels are designed mainly for axial load due to supporting floor slabs, a value of 900 plf (13.14 kN/m) was chosen to represent the design axial load. This load equals load carried by an external load-bearing wall carrying a two-story building and supporting a floor slab of 12 ft by 12 ft (3600 mm × 3600 mm) subjected to live load of 100 psf (5 kN/m$^2$). This design load was recommended by The Engineered Wood Association (APA) design guide [23].

### 3.2. Experimental results and discussion

The overall behavior of CSIP wall panels can be summarized as follows: the three panels exhibited an elastic behavior until loads of 3.85 kip (17 kN), 4.5 kip (20 kN), and 4.28 kip (19 kN) for panel 1, panel 2, and panel 3 respectively. When loading was continued, the panels started bending, and the facesheets in compression started to swell out near the supports, which caused debonding of facesheets. Upon further increase of the load, panels were unable to sustain further load (Fig. 9). In other words, panels failed by localized debonding between the core and facesheets in the maximum compression side. This mode of failure is known as wrinkling of the facesheet in compression which is caused by a sudden local buckling of the facesheets.

Lateral deflection at the mid-height of the panels versus the eccentric load is plotted in Fig. 10. As seen from the figure, load versus deflection curves were linear up to loads of 3.85 kip (17 kN), 4.5 kip (20 kN), and 4.28 kip (19 kN) for panel 1, panel 2, and panel 3, respectively, indicating the elastic behavior. At the onset of debonding, a change in the slope of load versus deflection curves was observed. Deflections recorded at this stage were 0.04 in. (1.0 mm), 0.059 in. (1.5 mm), 0.047 in. (1.2 mm) for panel 1, panel 2 and panel 3, respectively. The sudden drop in the load–deflection curves, at load of 6 kip (27 kN) for panels 1 and 2 and at load of 5.63 kip (25 kN) for panel 3, represents the failure of the panels in which panels could not sustain further

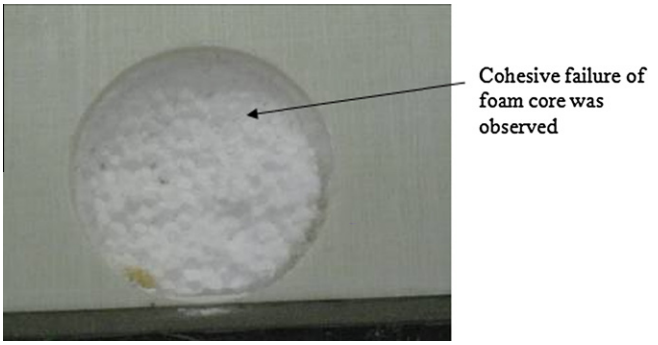


**Fig. 5.** Failure mode of CSIP for spray and film adhesives.

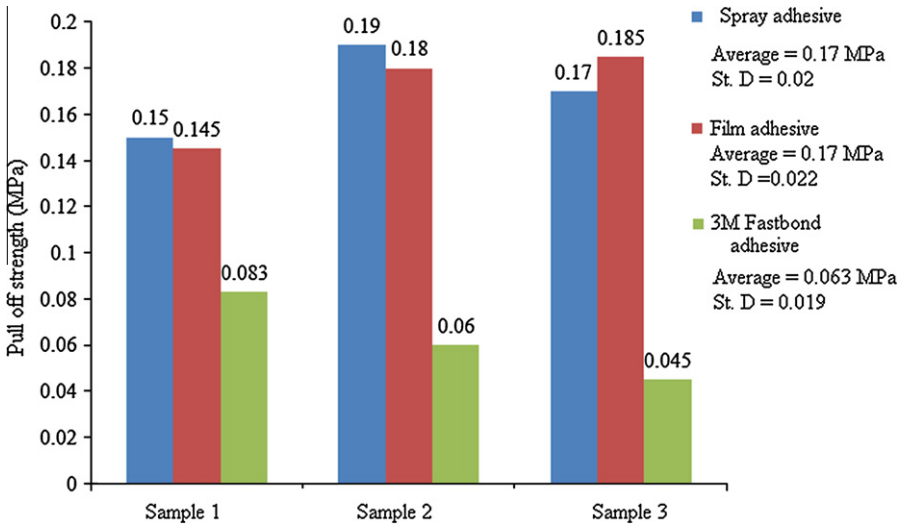


**Fig. 6.** Average pull-off strengths of the different adhesive.

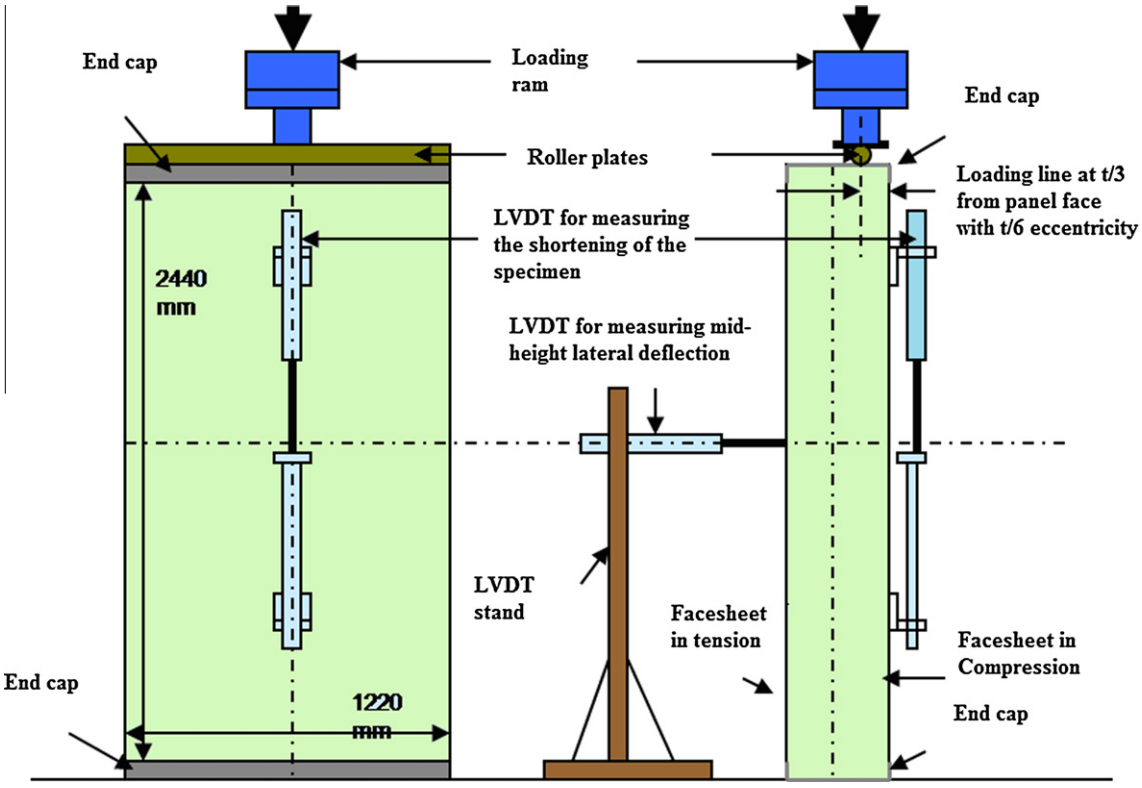


**Fig. 7.** Schematic for the experimental setup for the wall test according to ASTM E-72.

load. At these loads the unloading stage started. Deflections recorded at the peak load were 0.28 in. (7 mm), 0.12 in. (3 mm), and 0.08 in. (2 mm) for panel 1, panel 2, and panel 3; respectively. A total panel deflection of 1.06 in. (27 mm) was recorded at the end of the loading cycle. For panel 2, the loading was halted at the failure load based on the assumption that the unloading behavior of the panel 2 would be similar to that of panel 1. This can be noticed by the dotted line in Fig. 10 for panel 2 which shows the hypothetical unloading stage. However, for panel 3, the unloading stage was continued until the end of the loading cycle. As seen from Fig. 10, the behavior of panel 3 is similar to that of panel 2 with little difference in the failure load (i.e., 27 kN for panel 2 and 25 kN for panel 3). As seen from the load–deflection curve, the three panels could sustain the design load of 3.6 kip (16 kN) which is less than the load at the onset debonding for each panel. This satisfies the strength criteria. Further, deflections recorded at the onset of debonding for each panel were less than the allowable limit recommended by ACI 318 [24] which is $L/150$ (2438 mm/150 = 16.25 mm). Thus, the deflection criterion is also satisfied.

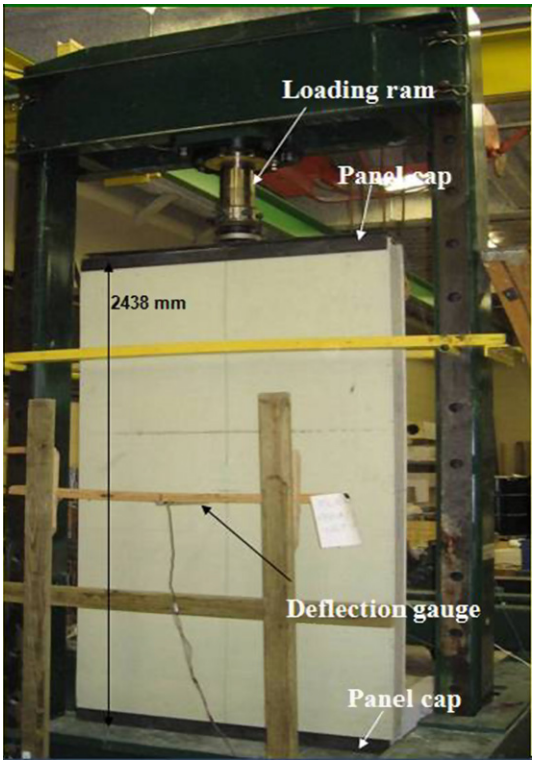


**Fig. 8.** CSIP wall testing under in-plane loading according to ASTM-E-72-05 [22].

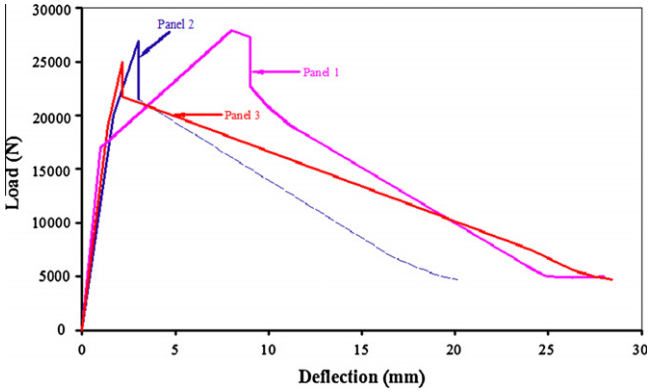


**Fig. 10.** Eccentric load versus lateral deflection at mid-height for CSIP wall panels (dotted line for panel 2 represents hypothetical unloading curve based on the assumption that the unloading behavior of panel 2 would be similar to that of panel 1).

Strains at various locations on the outer surfaces of facings were recorded using strain gauges. Gauges were mounted at both sides of the panel in the direction of loading (Fig. 11). Load–strain curves recorded at the mid-height of panels are shown in Fig. 12. The strains for panels 1 and 2 were very similar and their average values are plotted in Fig. 12. The strains in both panels (1 and 2) were almost identical till the failure load. However, the testing was stopped for panel 2 due to safety reasons upon impending failure. So the unloading strain for panel 2 was assumed to be the same as that of panel 1. As seen from Fig. 12, linear behavior was observed from load–strain curves till the peak load was attained. Changes in the slopes of the curves were observed at load 3.85 kip (17 kN) which indicated the initiation of debonding. Since compressive loading was eccentric, strains recorded in the compression sides were much higher than those recorded on the other side. The high strain values on the facesheets generated higher strains at the interface, which in turn resulted in debonding between the core and the facesheet along the unsupported length of the wall panels. Theoretically and according to a load eccentricity of $d/6$, maximum compressive strains at one side and no strain at the other side should have developed. However, small tensile strains were produced on the other side due to little errors in applying loading and boundary conditions. After unloading the panels, the strains on both sides were not zero at

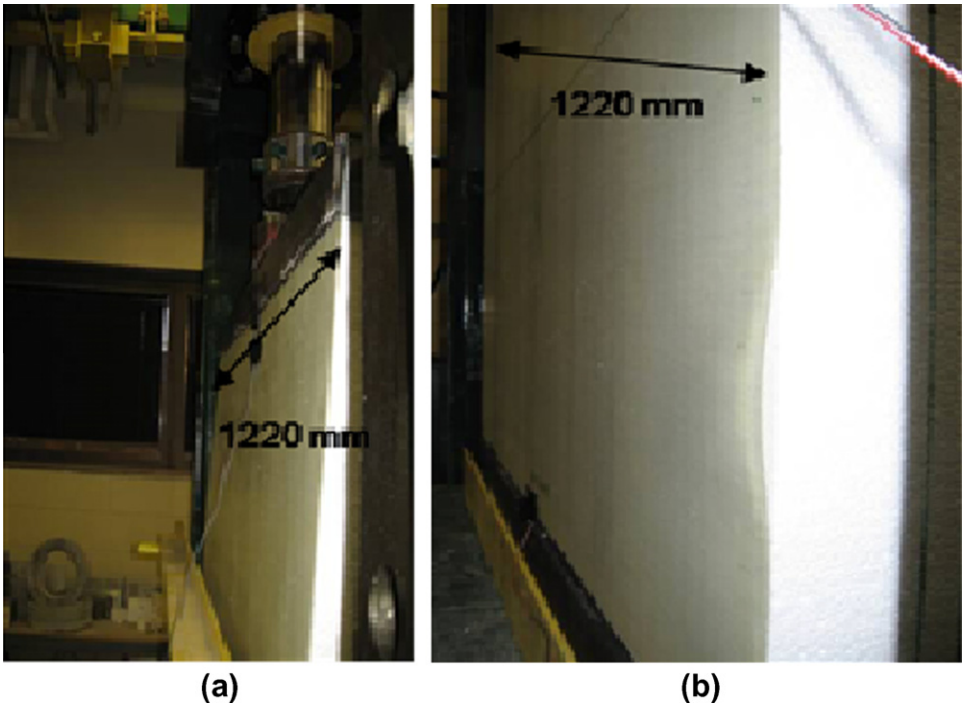


**Fig. 9.** Failure of CSIP wall panels: (a) elastic range, (b) failure of by debonding.

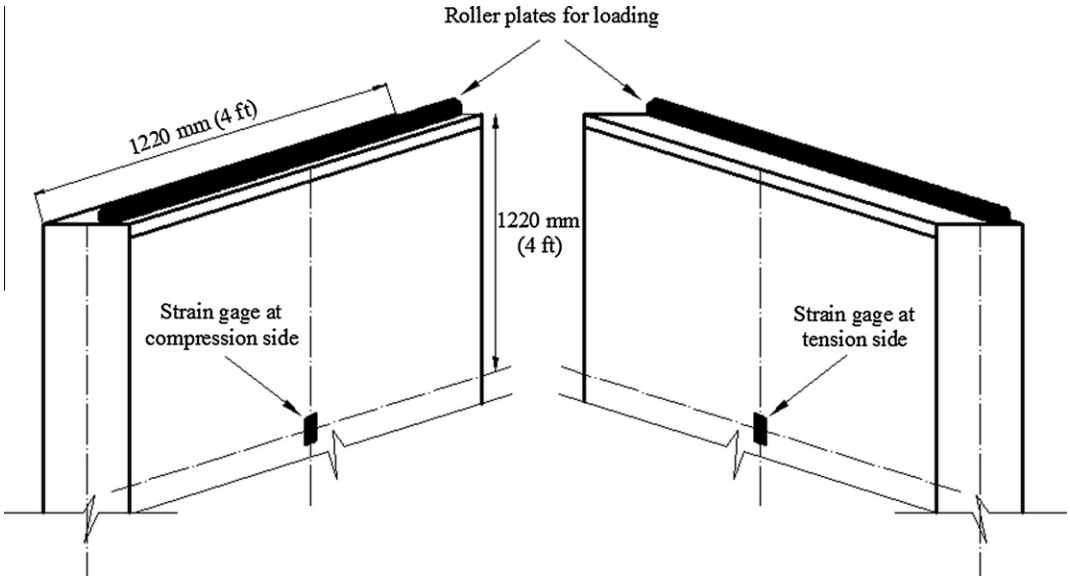


**Fig. 11.** Locations of strain gauges (SGs) on both sides of the CSIP wall panels (figure not to scale).

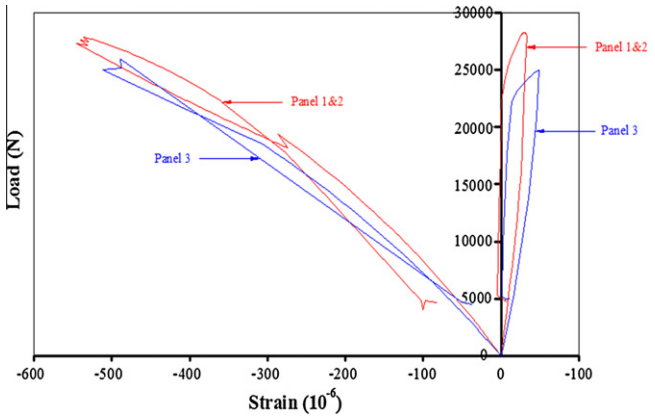


**Fig. 12.** Load versus strain at the mid-height of the panel.

the end of the testing event. This was due to the permanent set of the panel once the load was removed.

## 4. Analytical procedure

In general, there are two main criteria control the design of the sandwich panel; strength and deflection. As observed in the experiment, CSIP walls failed by facesheet/core debonding in the compression side which is related to strength. Deflection prior to debonding is also another issue that was checked with the building code limit. In the theoretical analysis presented in this section, models for stresses at debonding and deflection were developed. Stresses at facesheet/core debonding were modeled based on the Winkler foundation model whereas deflection was calculated using the ACI-318 [24] deflection formula for structural wall. To calculate the deflection for a CSIP wall, a formula for the equivalent stiffness of the CSIP sandwich wall panel considering the effect of the core deformations was developed.

### *4.1. Stresses at the facesheet/core debonding*

During loading of the sandwich wall panel, two types of stresses were developed at the facesheet in the compression side: the first

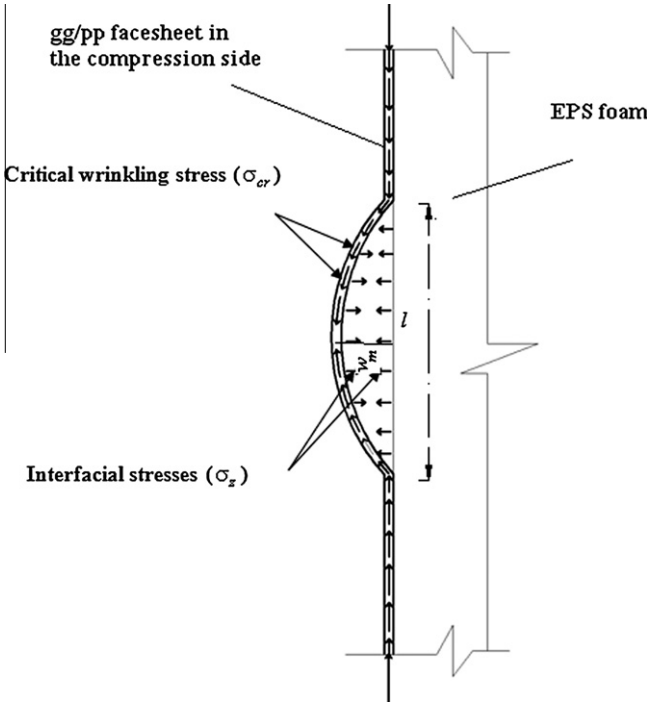


**Fig. 13.** Types of stresses developed at the compressive side of CSIP wall panel.

is a tensile out-of-plane stress at facesheet/core interface "$\sigma_z$" while the other is a compressive critical wrinkling stress in the facesheet of the debonded part "$\sigma_{cr}$" (Fig. 13). The debonding occurs when the tensile stress at the facesheet/core interface "$\sigma_z$" exceeds the tensile strength of the core material (e.g., EPS foam). As far as the wrinkling or debonding is concerned, there are three main categories known as: Case I: rigid base (single-sided), Case II: antisymmetrical and Case III: symmetrical. Case I occurs in the case of a sandwich panel under pure bending moment or a wall panel under eccentric loading in which the debonding is likely to occur at one side only. Cases II and III occur in the case of wall panels subjected to in-plane axial loads. Detailed explanation for the three cases can be found in Allen's book [12]. Since the CSIP wall panels

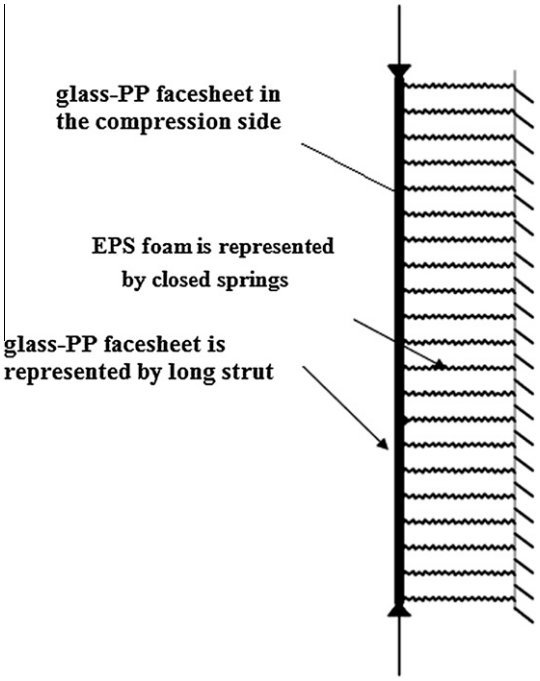


**Fig. 14.** Winkler foundation model for CSIP.

were subjected to eccentric loading, Case I was the mode of failure as demonstrated in the experiment.

The glass-PP facesheets under compression can be modeled as a strut or beam supported by an elastic foundation represented by the EPS foam core. In other words, CSIP wrinkling can be modeled as a Winkler foundation. In the analysis of the behavior of a long strut or beam supported by a continuous elastic medium; the medium can be replaced by a set of closed-spaced springs (Fig. 14); this phenomenon is normally known as the Winkler hypothesis, where the facesheet in this case is called Winkler beam while the core is known as the Winkler foundation. For a beam supported by a Winkler foundation, the governing differential equation of the beam is given as:

$$D_f \frac{d^4w}{dx^4} + P\frac{d^2w}{dx^2} + b\sigma_z = 0 \tag{1}$$

where $D_f$ is the flexural stiffness of the beam (facesheet), $P$ is axial load developed in the facesheet due to loading, $w$ is the displacement of the debonded part in $z$-direction. $\sigma_z$ is the interfacial tensile stress at facesheet/core interface, and $b$ is the width of the facesheet.

*4.1.1. Interfacial tensile stress ($\sigma_z$)*

Assume the springs' (foundation) stiffness is represented by a coefficient $k$. This coefficient represents the force needed to displace the springs in a unit area of the $xy$-plane through a unit displacement in the $z$-direction. Suppose this strut buckles into sinusoidal waves with half-wavelength of $l$ which is equal to the debonded length (Fig. 13), the displacement of the buckled portion in the $z$-direction can be expressed as:

$$w(x) = w_m \sin\frac{\pi x}{l} \tag{2}$$

where $w_m$ is the maximum displacement of the debonded part (i.e., at $l/2$). As shown in Fig. 13, the corresponding out-of-plane stress (interfacial stress) that is required to displace this portion of facesheet is given by:

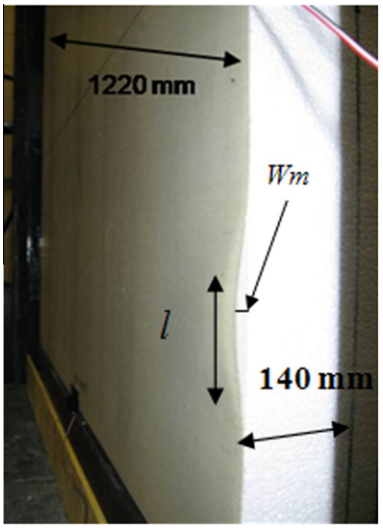


**Fig. 15.** Failure of CSIP wall panel under eccentric in-plane loading: Case I of Wrinkling ($wm$ = 10 mm, $l$ = core thickness = 140 mm).

$$\sigma_z = k \cdot w \tag{3}$$

From (2) and (3), we get:

$$\sigma_z = kw_m \sin\frac{\pi x}{l} \tag{4}$$

It should be mentioned that, as demonstrated by earlier studies [12,25,26], that the half-wavelength ($l$) of the debonded part is always of the same order as the thickness of the core. A similar observation was made in this study, when experimental testing demonstrated that the debonded part is almost equal to the core thickness (see Fig. 15).

Several investigations have been conducted to model the foundation stiffness $k$, (i.e., Sleight and Wang [27], Niu and Talreja [28]). However, we are proposing in this study the foundation stiffness suggested by Allen [12] which includes the effect of the half-wavelength of the debonded facesheet as well as the wrinkling type unlike the previous models. It also used an isotropic core (i.e., EPS foam). The general equation for $k$ to represent the three cases of wrinkling can be expressed as:

$$k = \frac{E_c}{c}\theta^2 f(\theta) \tag{5}$$

From Eqs. (4) and (5), the tensile stress at the facesheet/core interface for a given displacement ($w_m$) and half-wavelength ($l$) for the debonded facesheet can be given as:

$$\sigma_z = \frac{E_c}{c}\theta^2 f(\theta) w_m \sin\frac{\pi x}{l} \tag{6}$$

For Case I, referring to the control failure case in this study, $f(\theta)$ can be given by:

$$f(\theta) = \frac{2}{\theta}\frac{(3-\upsilon_c)\sinh\theta\cosh\theta + (1+\upsilon_c)\theta}{(1+\upsilon_c)(3-\upsilon_c)^2\sinh^2\theta - (1+\upsilon_c)^3\theta^2} \tag{7}$$

As noticed from Eq. (6), the interfacial stress is independent of the facesheet properties whereas it depends only on the core properties as well as core thickness. $\theta$ is a function of the core thickness and half-wavelength of $l$ and is given by $\frac{\pi c}{l}$. $f(\theta)$ is a function of core Poisson's ratio and $\theta$, and it has a different equation for each case of wrinkling.

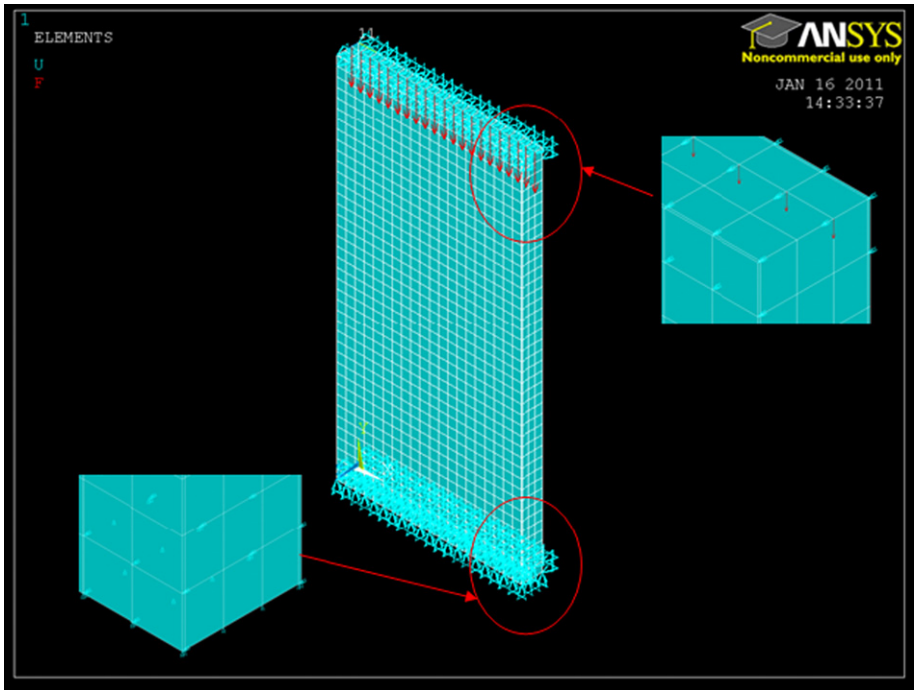


**Fig. 16.** CSIP wall model with loading and boundary conditions.

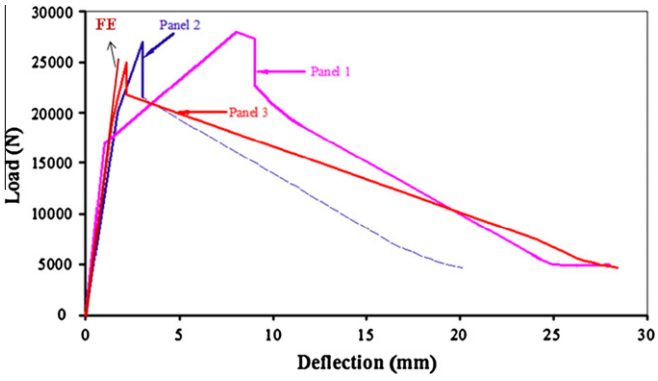


**Fig. 17.** Experimental and FE load–deflection curves at the mid-height of the panel.

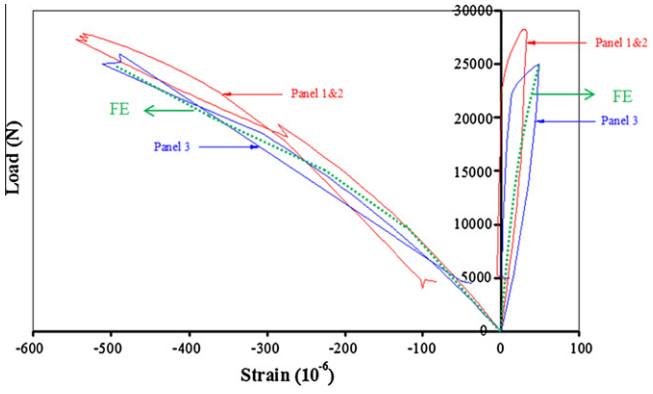


**Fig. 18.** Experimental and FE load–strain curves at the mid-height of the panel.

*4.1.2. Critical wrinkling stress in the compressive facesheet ($\sigma_{cr}$)*

The second stress that is associated with the debonding is the critical wrinkling stress in the facesheet in compression ($\sigma_{cr}$). This is a compressive in-plane stress developed in the facesheet due to loading. To model this stress ($\sigma_{cr}$), the analysis is based also on the Winkler beam model presented above. Substitution of $w(x)$ from Eq. (2) and ($\sigma_z$) from Eq. (6) into Eq. (1) and rearranging the equation, yields:

$$P\frac{\pi^2}{l^2} = b\frac{E_c}{c}\theta^2 f(\theta) + D_f\frac{\pi^4}{l^4} \tag{8}$$

For orthotropic facesheets, referring to glass-PP facesheet laminates, $D_f$ is given by

$$D_f = \frac{bE_f t^3}{12}\left(1-\upsilon_{xy}^2\right) \tag{9}$$

where $\upsilon_{xy}$ is the Poisson's ratio of the facesheet in the $xy$-plane. This will consider the through thickness anisotropy effect due to the orthotropic facesheets. Dividing Eq. (8) by $bt$ and substituting of $D_f$, $\frac{\pi}{l}=\frac{\theta}{c}$, recognizing that the wrinkling compressive stress in the facesheet ($\sigma_{cr}$) is given as $P/bt$, this yields:

$$\sigma_{cr} = \frac{E_c}{t}cf(\theta) + \frac{E_f}{12}\left(\frac{\theta}{c}\right)^2 t^2\left(1-\upsilon_{xy}^2\right) \tag{10}$$

As seen in Eq. (10), the critical wrinkling stress ($\sigma_{cr}$) is a function of the properties and thicknesses of facesheet and core unlike the interfacial tensile stress ($\sigma_z$) which is independent of the facesheet properties and mainly depends on the core material.

Several investigations were conducted to predict the critical wrinkling stress for all wrinkling cases. Most of these studies have led to empirical formulas. All the formulas take the following form for sandwich panels with solid cores (such as EPS foam):

$$\sigma_{cr} = \beta(E_f E_c G_c)^{1/3} \tag{11}$$

The value of the constant $\beta$ in Eq. (11) has been suggested by various investigators (0.79 and 0.63 by Gough et al. [14], 0.76 by Cox et al. [29], 0.91 and 0.5 by Hoff and Mautner [15], 0.825 by Plantema [30]). From this discussion, it can be seen that there

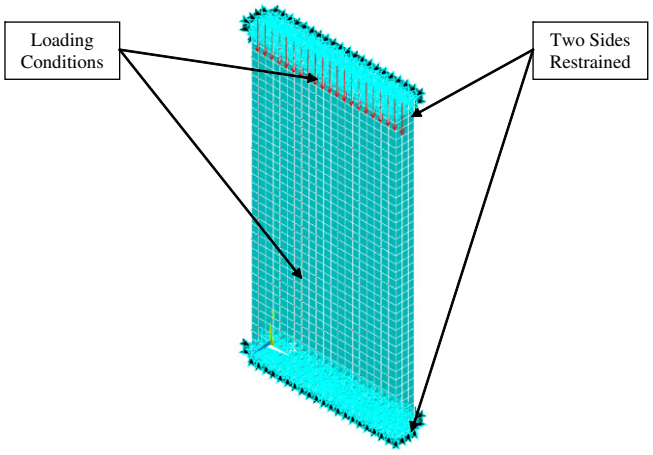


**Fig. 19.** Structural CSIP wall panel with loading and boundary conditions.

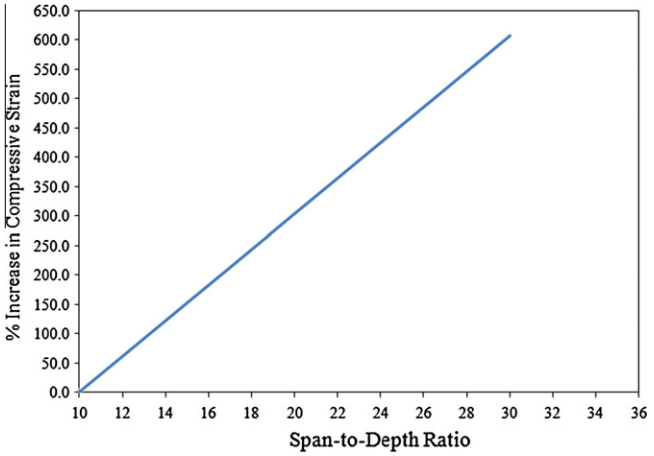


**Fig. 21.** Relationship between the span-to-depth ratio and % of increase in facesheet compressive strain.

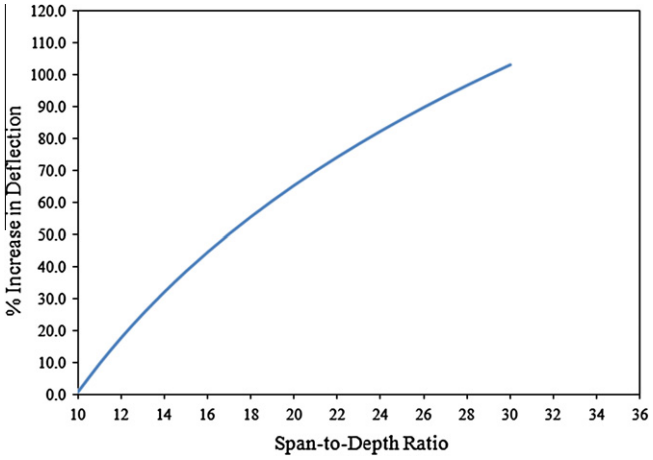


**Fig. 20.** Relationship between the span-to-depth ratio and % of increase in deflection.

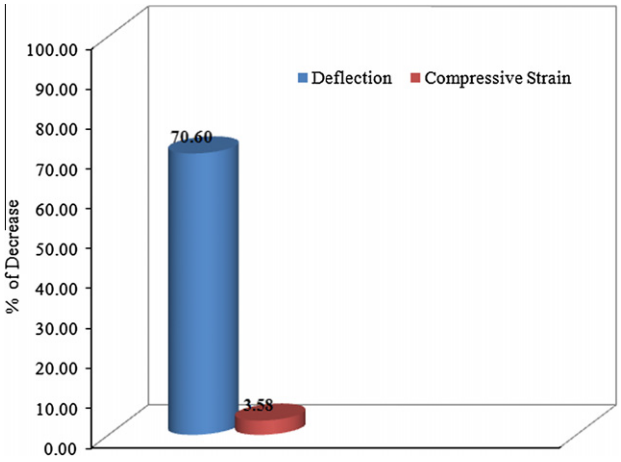


**Fig. 22.** Percentage of decrease in deflection and facesheet compressive strain (from 1 PCF foam core to 3 PCF foam core).

**Table 4**
Experimental, theoretical, and FE deflections at initiation of debonding.

| Data | Experimental deflection at debonding in. (mm) | Theoretical deflection in. (mm) | FE deflection in. (mm) |
|---|---|---|---|
| Panel 1 | 0.04 (1.0) | 0.035 (0.89) | 0.049 (1.25) |
| Panel 2 | 0.059 (1.5) | 0.042 (1.06) | 0.049 (1.25) |
| Panel 3 | 0.047 (1.2) | 0.04 (1.0) | 0.049 (1.25) |

are different approaches regarding the calculation of the wrinkling stress in the compressive facesheet. Further, most of these studies considered only isotropic facesheets when the sandwich panels used to have isotropic facesheets made of metal. In this study, the model derived for the wrinkling stress in this study is taking into consideration the orthotropic facesheets and solid core.

Based on the critical wrinkling stress, the nominal load capacity ($P_n$) can be determined including the effect of the eccentricity. From the theory of mechanics, the stresses under combination of compressive normal force and moment is given by:

$$\sigma = \frac{P_n}{A} \pm \frac{M \cdot y}{I} \tag{12}$$

The above equation can be rewritten in terms of debonding load ($P_n$), facesheet thickness ($t$), panel thickness ($d$), face thickness and eccentricity ($e = d/6$) as follows:

**Table 5**
FE study parameters.

| Item | Values |
|---|---|
| Span-to-depth ratio | 10, 12, 16, 15, 18, and 24 |
| Core density | 1 PCF and 3 PCF |

$$\sigma = \frac{P_n}{2 \cdot b \cdot t}\left[1 \pm \frac{6 \cdot e}{d}\right] \tag{13}$$

By substituting in the above equation for $e$ equal to $d/6$, as in the experiment, the maximum compressive load, which corresponds to the critical wrinkling stress, can be analytically obtained as follows:

**Table 6**
Parametric study table for CSIP wall panels.

| Panel # | Panel's name | Span (ft) | Core thickness (in.) | Core density (PCF) | Span/depth ratio |
|---|---|---|---|---|---|
| 1 | CSIP8101 | 8 | 10 | 1 | 10 |
| 2 | CSIP881 | 8 | 8 | 1 | 12 |
| 3 | CSIP861 | 8 | 6 | 1 | 16 |
| 4 | CSIP12101 | 12 | 10 | 1 | 15 |
| 5 | CSIP1281 | 12 | 8 | 1 | 18 |
| 6 | CSIP1261 | 12 | 6 | 1 | 24 |
| 7 | CSIP8103 | 8 | 10 | 3 | 10 |
| 8 | CSIP883 | 8 | 8 | 3 | 12 |
| 9 | CSIP863 | 8 | 6 | 3 | 16 |
| 10 | CSIP12103 | 12 | 10 | 3 | 15 |
| 11 | CSIP1283 | 12 | 8 | 3 | 18 |
| 12 | CSIP1263 | 12 | 6 | 3 | 24 |

**Table 7**
Results for 1 PCF core and 8 ft span.

| Panel's name | Span/depth ratio | Deflection (mm) | Compressive strain in facesheet (MPa) | % Increase in deflection | % Increase in strain |
|---|---|---|---|---|---|
| CSIP8101 | 10 | 9.13 | $-0.293 \times 10^{-4}$ | 0 | 0 |
| CSIP881 | 12 | 10.96 | $-0.462 \times 10^{-4}$ | 20.04 | 57.68 |
| CSIP861 | 16 | 13.6 | $-0.763 \times 10^{-4}$ | 48.96 | 160.4 |

**Table 8**
Results for 1 PCF core and 12 ft span.

| Panel's name | Span/depth ratio | Deflection (mm) | Compressive strain in facesheet (MPa) | % Increase in deflection | % Increase in strain |
|---|---|---|---|---|---|
| CSIP12101 | 15 | 20.75 | $-0.371 \times 10^{-4}$ | 0 | 0 |
| CSIP1281 | 18 | 24.6 | $-0.596 \times 10^{-4}$ | 18.6 | 60.65 |
| CSIP1261 | 24 | 29.6 | $-0.108 \times 10^{-3}$ | 42.65 | 191.1 |

**Table 9**
Results for 10, 12 and 16 span-to-depth ratios and 8 ft span.

| Panel's name | Core density (PCF) | Deflection (mm) | Compressive strain in facesheet (MPa) | % Decrease in deflection | % Decrease in strain |
|---|---|---|---|---|---|
| CSIP8101 | 1 | 9.13 | $-0.293 \times 10^{-4}$ | 0 | 0 |
| CSIP881 | 1 | 10.96 | $-0.462 \times 10^{-4}$ | 0 | 0 |
| CSIP861 | 1 | 13.6 | $-0.763 \times 10^{-4}$ | 0 | 0 |
| CSIP8103 | 3 | 2.43 | $-0.266 \times 10^{-4}$ | 73.3 | 8.5 |
| CSIP883 | 3 | 3.00 | $-0.461 \times 10^{-4}$ | 72.6 | 2.16 |
| CSIP863 | 3 | 3.97 | $-0.698 \times 10^{-4}$ | 70.81 | 8.52 |

**Table 10**
Results for 15, 18 and 24 span-to-depth ratios and 12 ft span.

| Panel's name | Core density (PCF) | Deflection (mm) | Compressive strain in facesheet (MPa) | % Decrease in deflection | % Decrease in strain |
|---|---|---|---|---|---|
| CSIP12101 | 1 | 20.75 | $-0.371 \times 10^{-4}$ | 0 | 0 |
| CSIP1281 | 1 | 24.6 | $-0.596 \times 10^{-4}$ | 0 | 0 |
| CSIP1261 | 1 | 29.6 | $-0.108 \times 10^{-3}$ | 0 | 0 |
| CSIP12103 | 3 | 5.90 | $-0.331 \times 10^{-4}$ | 71.66 | 10.78 |
| CSIP1283 | 3 | 7.41 | $-0.563 \times 10^{-4}$ | 69.96 | 5.55 |
| CSIP1263 | 3 | 10.00 | $-0.103 \times 10^{-3}$ | 51.81 | 4.6 |

$$\sigma_{cr} = \frac{P_n}{2 \cdot b \cdot t}\left[1 + \frac{6 \cdot (d/6)}{d}\right] = \frac{P_n}{b.t} \tag{14}$$

Therefore, the nominal load capacity is given by:

$$P_n = \sigma_{cr} \cdot b \cdot t \tag{15}$$

### 4.2. Deflection

Deflection of the sandwich wall is calculated based on the equivalent stiffness to consider the core shear deformations. Thus, the equivalent stiffness ($D_{equiv.}$) of a CSIP sandwich panel should be determined first. As mentioned earlier, failure modes of sandwich walls include global buckling and local buckling "wrinkling" which can either be debonding or core crushing. The full-scale CSIPs wall panels failed by facesheet/core debonding. As far as the global buckling, a theoretical formula was developed by the authors for the CSIP walls global buckling considering the core deformations. The formula also took into consideration the nature of the glass-PP facesheet which is orthotropic as well as the EPS core which is isotropic. Tests were conducted on reduced scale panels to ensure global buckling failure without any kind of debonding. The

formula can also be used for large scale panels as long as there is no debonding or wrinkling. For the sake of brevity, the basis of the derivation of this formula is not presented here but can be found elsewhere [12]. The formula of the global buckling load of the CSIP wall is given as:

$$P = \frac{\pi^2}{L^2}\frac{E_f I}{\left(1+\frac{\pi^2 E_f I\left(1-\upsilon_{xy}^2\right)}{L^2\cdot b\left(\frac{d+c}{2}\right)\cdot G}\right)}\left(1-\upsilon_{xy}^2\right) \tag{16}$$

Again, the term $(1-\upsilon_{xy}^2)$ is to consider the orthotropic facesheet, referring to glass-PP. According to Euler formula, the global buckling load ($P_E$) for a compression member made of a homogenous materials is given by:

$$P_E = \frac{\pi^2}{L^2}\cdot D \tag{17}$$

where $D$ is the member's flexural stiffness which expressed as $EI$ for a homogenous element (i.e., made of one material). Comparing Eq. (16) by Eq. (17), the equivalent stiffness for a sandwich panel with an orthotropic facesheet and solid core can be expressed as:

$$D_{equiv.} = \frac{E_f I}{\left(1+\frac{\pi^2 E_f I\left(1-\upsilon_{xy}^2\right)}{L^2\cdot b\left(\frac{d+c}{2}\right)\cdot G}\right)}\left(1-\upsilon_{xy}^2\right) \tag{18}$$

As noticed in Eq. (18), $D_{equiv.}$ takes into consideration deformation of the core in terms of shear area and core shear modulus as well as the orthotropic nature of glass-PP facesheets in terms of the in-plane Poisson's ratio ($\upsilon_{xy}$). The equivalent stiffness given by Eq. (18) is also used to obtain the deflection of a sandwich wall panel subjected to in-plane loading. Wall deflection at the mid-height is determined according to ACI-318 [24] as:

$$\Delta = \frac{(5M)L^2}{48(D)_{equiv.}} \tag{19}$$

where,

$$M = \frac{M_{sa}}{1-\frac{5P_s L^2}{48(D)_{equiv.}}} \tag{20}$$

Eq. (20) takes into consideration the second order deflection or P-delta effect due to the compressive load where $P_s$ is applied in-plane eccentric loading and $M_{sa}$ is the applied moment at the mid-height of the panel due to that load ($P_s$). $(D)_{equiv.}$ is determined using Eq. (18). It should be noted that Eq. (20) is applicable only up to onset of debonding, i.e., linear stage only. Therefore, loads used to determine the moments were those at the imitation of debonding.

## 5. Validation of the experimental results

### 5.1. Stresses at debonding

#### 5.1.1. Interfacial tensile stress ($\sigma_z$)

As shown in Fig. 17, the half-wavelength is almost equal to the core thickness (140 mm) and the maximum out-of-plane displacement of the debonded facesheet is almost 10 mm for both panels. Therefore, the function $\theta$ can be determined as follows:

$$\theta = \frac{\pi c}{l} = \frac{\pi(140)}{140} = 3.14$$

As observed in the experimental; $w_m$ (10 mm) represents 7% of the core thickness, $c = l$, $\sin\frac{\pi x}{l}$ = unity since the stress is calculated at the middle. Accordingly, and for the design purpose, Eq. (6) can be rewritten as:

$$\sigma_z = 0.07\pi^2 f(\theta) E_c \tag{21}$$

$f(\theta)$ is determined according to Eq. (7):

$$f(\theta) = \frac{2}{3.14}\frac{(3-0.25)\sinh(3.14)\cosh(3.14)+(1+0.25)(3.14)}{(1+0.25)(3-0.25)^2\sinh^2(3.14)-(1+0.25)^3(3.14)^2} = 0.191$$

Thus, the interfacial out-of-plane stress can be then determined from Eq. (21) as follows:

$$\sigma_z = 0.07\pi^2(0.191)(1.2) = 0.16\ \text{MPa} = 23.8\ \text{psi}$$

As seen from Table 2, the maximum tensile strength of the EPS core is 0.138 MPa (20 psi). As previously mentioned, the debonding occurs when the interfacial stress exceeds the tensile strength of the core material. As demonstrated from the model, the out-of-plane stress (23.8 psi) has exceeded the tensile strength of the core material (20 psi) thereby initiating debonding failure as observed.

#### 5.1.2. Critical wrinkling stress ($\sigma_{cr}$)

As shown in Fig. 12, the compressive strains at failure are 0.00055 for panel 1 and panel 2, and 0.0005 for panel 3. These strains result in experimental wrinkling stresses as follows:

Panels 1 and 2:

$$\sigma_{cr\,\text{exp.}} = \varepsilon_{\text{exp.}}.E_f$$

$$\sigma_{cr\,\text{exp.}} = 0.00055(15,169) = 8.34\ \text{MPa}$$

Panel 3:

$$\sigma_{cr\,\text{exp.}} = 0.0005(15,169) = 7.58\ \text{MPa}$$

The theoretical wrinkling stress can be calculated using Eq. (10) as follows:

$$\sigma_{cr} = \frac{E_c}{t}cf(\theta) + \frac{E_f}{12}\left(\frac{\theta}{c}\right)^2 t^2\left(1-\upsilon_{xy}^2\right) = \frac{1.2}{3.04}(140)(0.191) + \frac{15,169}{12}\left(\frac{3.14}{140}\right)^2(3.04)^2(1-0.11^2) = 16.43\ \text{MPa}$$

Comparing the experimental values of the wrinkling stress (8.34 MPa and 7.58 MPa) with the theoretical value predicted by the proposed model (16.43 MPa), it can be noticed that the experimental value is almost one-half of the theoretical one. This was common for most of the previous work conducted on wrinkling stress (for example Hoff et al. [6], the theoretical constant went from 0.91 to 0.5 to fit the experimental results). Thus, these studies have proposed an empirical formula to correlate with the experiments.

In this case, the core has much lower mechanical properties compared to that of the facesheets in which the ratio of facesheet modulus to that of the core is the highest ratio used for a sandwich panel to date ($E_f/E_c$ = 12,500 in this study versus 1000 for other studies reported in the literature). It can be noticed that the critical wrinkling stress of the wall can be predicted using Eq. (11) with $\beta$ = 0.25. Accordingly, to fit the experimental results, the following empirical formula is proposed to predict the wrinkling stress of the CSIPs taking into consideration the orthotropic facesheets:

$$\sigma_{cr} = 0.25(E_f E_c G_c)^{1/3}\left(1-\upsilon_{xy}^2\right) \tag{22}$$

By comparing the proposed constant (0.25) with the other constants previously proposed for sandwich structures, it can be noticed that this constant is smaller than the ones that have been used before. The main reasons for this include the orthotropic facesheet used in the study and the high moduli ratio of the facesheet and core. If the $\sigma_{cr}$ is calculated using Eq. (22), we will obtain 8.25 MPa which is close to the experimental values (8.34 MPa and 7.58 MPa).

Further, Eq. (15) can be used to calculate the approximation for nominal in-plane load capacity for the CSIP wall panels. By substituting in Eq. (15), one can find that the nominal load capacities are 30.9 kN for panels 1 and 2, and 28.1 kN for panel 3. Comparing these values with the experimental failure loads (27 kN for panels 1 and 2 and 25 kN for panel 3), it is clear that Eq. (15) could predict the failure load.

### 5.2. Deflection

To calculate the deflection, the equivalent stiffness of the CSIP wall was calculated using Eq. (18) then the deflection was calculated using Eq. (19) at the mid-height of the panel. Table 4 summarizes the results of these calculations. As seen from Table 4, the differences between the experimental and theoretical deflections are 12%, 29%, and 15% for panel 1, panel 2, and panel 3, respectively. This acceptable convergence validates the equivalent stiffness formula for CSIP wall as well as the analytical model for CSIP wall deflection.

### 5.3. Finite element modeling (FEM)

FEM for the panels was performed using ANSYS 12 software package [31] in which the glass-PP facesheets and EPS foam core were modeled using 3-D structural solid element, SOLID45. The element is defined by eight nodes having three degrees of freedom at each node consisting of translations in the nodal $x$, $y$, and $z$ directions. The element supports plasticity, creep, swelling, stress stiffening, large deflection, and large strain capabilities [31]. Since the glass-PP facesheets are bi-directional laminates, they were modeled as orthotropic material with nine properties whereas the EPS foam was considered as isotropic material. The nine properties required to define the orthotropic material are: modulus of elasticity ($E$) in the three directions, shear modulus in the three panels, and Poisson's ratio ($v$) in the three planes. These properties are listed in Table 1. A total of 4000 elements were obtained after meshing; including 1600 elements for the facesheets and 2400 elements for the core. The loading and boundary conditions were applied to the model to the actual ones. All the nodes on the bottom of the panel were constrained in the y direction whereas the top and bottom side nodes for a distance of 2.35 in. (60 mm) were constrained in the $z$ direction in order to represent the end caps. The load was distributed along the top line nodes located at $d/6$ from the panel center. A CSIP wall panel with loading and boundary conditions is shown in Fig. 16.

Nonlinear static analysis enabling large displacement was pursued in order to best simulate the response of the CSIP wall under in-plane eccentric loading. Loads were applied in small increments to avoid any convergence problems that might occur during the analysis. A total load of 6 kip (27 kN) was applied to the wall model. This load was divided into 27 load steps. A displacement convergence criterion was considered in the analysis. The failure occurred at load step 25 (i.e., corresponding to load 25 kN) after which the convergence did not occur and the panel was not able to withstand any further loading. Load deflection and load strain curves resulting from the FEM compared with those obtained from the experiment at the mid-height of the panel are shown in Figs. 17 and 18, respectively. As seen from the load–deflection curves, the behavior is almost identical till the initiation of debonding in which the difference in the deflection at that point (i.e., at load 20 kN) was 20% for panel 1, 19% for panel 2, and 4% for panel 3. In case of strain, the maximum compressive strain in the glass-PP facesheet as obtained from the FEM at the failure was 0.000485 which differs by 13% for panels 1 and 2 and by 3% for panel 3. This small difference validates the accuracy of the FE modeling in predicting the behavior of a CSIP wall member.

## 6. Parametric finite element study for CSIP walls

After verifying the accuracy of the FEM using experimental data for full-scale CSIP wall testing, the FEM was shown to be an effective tool in investigating the behavior of the proposed panels. Further, it can be used to study the response of CSIPs under different types of loading as well as boundary conditions. This section presents a comprehensive parametric finite element study on full-sized CSIP walls to be used for residential buildings. The study includes various effective parameters that can affect the behavior of CSIPs. The parametric study was conducted using ANSYS software package. Such parametric study will result in an effective design optimization of the proposed panels. This section begins by presenting the different parameters considered, and then discusses the loads and the FEM procedure. Lastly, it discusses the results to determine the effect of each parameter on the behavior of CSIPs to obtain the optimum design for the structural engineer.

### 6.1. Study parameters

There are many parameters that are expected to have a significant influence on the behavior and design of the CSIPs. The most effective parameters were optimized. The parameters included were span-to-depth ratio and core density. Furthermore, to be more realistic in the determining the effects of each parameter, different spans were used in the modeling. Table 5 lists the range of values of the considered parameters.

### 6.2. Loads

Wall panels are designed mainly for axial load in conjunction with transverse load due to wind or earthquake loads. Based on this, a value of 13.4 N/mm (900 plf) was chosen to represent the axial load that equals the load carried by an external load-bearing wall carrying a two-story building and supporting a floor slab of 3600 mm $\times$ 3600 mm (12 ft by 12 ft) subjected to a live load of 0.005 N/mm$^2$ (100 psf). In addition, 0.002 N/mm$^2$ (40 psf) was used to represent the transverse load coming from high wind loads. The wind loads were calculated based on the high wind (speed = 150 mph) acting on a two-story residential building located in a suburban area and existing on escarpment topography.

### 6.3. Finite element analysis (FEA)

Nonlinear static analysis by enabling large deflections was pursued for the panel models using ANSYS to determine the effect of the previously-mentioned parameters on the deflection as well as facesheet strains. The core and facesheets were modeled using SOLID 45 element. The finite element mesh for the panels was optimized, and the maximum size used for meshing was 60 mm (2.36 in.).

The loading and boundary conditions were adapted. The two sides of the panel that will be connected to the support were restrained for all translations only to express the real situation. The restraining for all translations and rotations is difficult to achieve in residential buildings, especially the connection between the floor and wall. A bearing length of 2.5 in. (60.5 mm) was used as the minimum support length recommended by most panelized construction manufacturers [32]. The transverse loads were applied on the top surface nodes of the panel whereas the in-plane eccentric loading for walls was at a distance of $d/6$ from the center of the panel as recommended by ASTM-72 [22]. Fig. 19 shows the typical models for floor and wall panel used in the parametric study with loading and boundary conditions.

A total of 12 models were analyzed for both wall and floor panels. Table 6 lists the parametric study models. It should be noticed that the panel name was written as follows: the first four letters stand for CSIP, the first number represents the span length in feet, the second number indicates the core thickness in inches, and the third number refers to core density in PCF.

### 6.4. Results and discussion

The results obtained through the FEM were the maximum deflections and the maximum compressive strains for the FE models since these are the most important outputs that control the design of the CSIPs. A comparison of these results was then conducted to investigate the effect of each parameter. The behavior of the panels was almost linear till the ultimate applied load.

#### 6.4.1. Span-to-depth ratio

The results of the considered span to depth ratio for 8 ft and 12 ft spans are listed in Tables 7 and 8. In these tables, the maximum deflection at mid-span and the maximum compressive strain at middle of the top facesheet are listed. The last two columns represent the percentage of increase for deflection and compressive strain in the top facesheets. As seen from Table 7, panel CSIP8101 recorded the lowest deflection and strain since it has the lowest span-to-depth ratio. When this ratio increases, the deflection and strain are expected to increase as well due to lower stiffness as the span-to-depth ratio increases. Furthermore, the increase in the strain was higher than that of the deflection indicating that the effect of the span-to-depth ratio has more impact on the strain. In addition and as shown in Table 8, when changing the span-to-depth ratio with the same rate, but longer span, the increase in the deflection was about the same as in 8 ft span. However, the gain in strain was higher because the effect of span is more significant than that of the thickness in the calculation of the strain for a sandwich panel. This is mainly because strain is proportional to the square of the span whereas the shear deflection, which is more than the bending deflection, is only proportional linearly to the span. Based on the average increases in both deflections and strains for both spans, Figs. 20 and 21 were developed to describe the relationship between the span-to-depth ratio and the percentage on increase in both deflection and strain, respectively.

#### 6.4.2. Core density

Tables 9 and 10 illustrate the results of models for the two spans, 8 and 12 ft, respectively. The percentage of decrease is calculated for the same span-to-depth ratio. As shown in the Tables, the deflections decreased significantly when increasing the core density from 1 PCF to 3 PCF. Further, the decrease in deflection and strains are almost similar for the two different spans. Furthermore, the decrease was not affected significantly by the span-to-depth ratio and or the span. Another notice can be drawn from these results is that decreases in strains were slightly affected compared to that of the deflections. This is because the strain depends on the dimensions and thicknesses of both the core and facesheet and not on the core density. The main conclusion of these results is that the core density (or shear rigidity) plays a significant role in the resulting deflection and has very little effect on the strain of the facesheets. Fig. 22 shows the average percentage of decrease in both deflection and compressive strain in the facesheet due to changing the core density from 1 PCF to 3 PCF.

## 7. Conclusions

The behavior of a new type of composite panels (CSIPs) for structural wall applications was investigated under eccentric compressive loading. Analytical and finite element models were also provided to model this behavior. In addition, a parametric finite elements study was conducted to investigate the key design parameters on the behavior of CSIP wall panels. The parameters considered were span-to-depth ratio and core density. The following conclusions are drawn from this study:

1. CSIPs panels failed by localized debonding between the core and facesheets in the maximum compression side with natural half-wavelength equal to the core thickness. This mode of failure is known as wrinkling of the facesheet in compression which is caused by a sudden local buckling of the facesheets. This mode is mainly because the out-of-plane interfacial stress exceeded the core tensile strength. This was demonstrated also by the pull off strength tests.
2. The behavior of the panels was linearly elastic till the onset of debonding. After the initiation of debonding, panels showed a decrease in the stiffness and this was observed from the change of the slopes of the load–deflection curves.
3. Despite the debonding, CSIPs wall panels satisfied both design load and deflection limit as provided by APA design guide and ACI-318, respectively. In other words, they have satisfied both strength and stiffness criteria required for design of a structural sandwich panel.
4. A model for the interfacial facesheet/core out-of-plane tensile stress was developed and validated by demonstrating the close proximity to the experimental results. The results proved that the predicted interfacial stress is higher than core tensile strength and therefore, debonding was the general mode of failure. This validates the criteria that the interfacial stress in independent of loading and boundary conditions and depends only on the core properties.
5. The proposed theoretical model for the critical wrinkling stress based on the Winkler foundation model less conservatively predicted the actual wrinkling stress. Accordingly, an empirical formula in Eq. (22) was proposed to predict the critical wrinkling stress at the debonding for CSIP wall panels considering the orthotropic facesheets with $P_n = \sigma_{cr} \cdot b \cdot t$.
6. A formula for equivalent stiffness of sandwich wall panel with orthotropic facesheet and solid core was developed to take into consideration the effect of core deformation. This formula is used to determine the deflection of sandwich wall. The close convergence between the experimental and theoretical deflections validates this formula.
7. The reasonable agreement between the analytical and finite element models and experimental results for CSIP walls illustrates that the analytical model accurately predicts the performance of the panel and is likely to minimize full scale tests of panels for code acceptance. In addition, a modeling tool would also allow the behavior of the panels to be investigated under different load combinations.
8. Parametric study developed using FE modeling showed that the span-to-depth ratio is an effective parameter for both deflection and compressive strain in the facesheet whereas the core density has a significant influence on the deflection and very little effect on the compressive strain of the facesheet. The deflection decreased by 70% due to changing the core density from 1 PCF to 3 PCF whereas as a small reduction in strain (about 3%) was obtained. This is because the strain depends mainly on the dimensions and thicknesses of both core and facesheet not on the core rigidity.

## Acknowledgments

The authors gratefully acknowledge funding and support provided by National Science Foundation (NSF) for this research

project (CMMI-825938). They also would like to thank Dr. Amol Vaidya for his help in experimental results.

## References

[1] Zenkert D. An introduction to sandwich construction. West Midlands, United Kingdom: Engineering Materials Advisory Service Ltd; 1995.
[2] Mousa Mohammed. Optimization of structural panels for cost-effective panelized construction. MS Thesis. University of Alabama at Birmingham: CCEE Department; 2007.
[3] Khotpal Amol. Structural characterization of hybrid fiber reinforced polymer (FRP)-autoclaved aerated concrete (AAC) panels. MS Thesis. University of Alabama at Birmingham: CCEE Department; 2004.
[4] Shelar Kedar. Manufacturing and design methodology of hybrid fiber reinforced polymer (FRP)-autoclaved aerated concrete (AAC) panels and its response under low velocity impact. MS Thesis. University of Alabama at Birmingham: CCEE Department; 2006.
[5] Uddin N, Fouad H. Structural behavior of FRP reinforced polymer-autoclaved aerated concrete panels. ACI Struct J 2007;104(6):722–30.
[6] Vaidya Amol S. Lightweight composites for modular panelized construction. PhD Dissertation. University of Alabama at Birmingham: CCEE Department; 2009.
[7] Mousa MA, Uddin N. Experimental and analytical study of carbon fiber-reinforced polymer (FRP)/autoclaved aerated concrete (AAC) sandwich panels. J Eng Struct 2009;31:2337–44.
[8] Chevali Venkata S. Flexural creep of long fiber thermoplastic composites: effect of constituents and external variable on non-linear viscoelasticity. PhD Dissertation. University of Alabama at Birmingham: ME Department; 2009.
[9] Daniel IM, Gdoutos EE, Wang KA, Abot JL. Failure modes of composites sandwich beams. Int J Damage Mech 2002;11:309–34.
[10] Gdoutos EE, Daniel IM, Wang K-A. Compression facing wrinkling of composite sandwich structures. J Mech Mater 2003;35:511–22.
[11] Kardomateas George A. Global buckling of wide sandwich panels with orthotropic phases. In: Proceeding of the 7th international conference on sandwich structures. Aalborg University; 2005.
[12] Allen HG. Analysis and design of structural sandwich panels. London, United Kingdom: Pergamon Press Ltd; 1969.
[13] Galletti GaetanoG, Vinquist Christine, Es-said OmarS. Theoretical design and analysis of a honeycomb panel sandwich structure loaded in pure bending. J Eng Fail Anal 2007;15:555–62.
[14] Gough GS, Elam CF, de Bruyne ND. The stabilization of a thin sheet by a continuous supporting medium. J Roy Aeronaut Soc 1940;44:12–43.
[15] Hoff NJ, Mautner SF. The buckling of sandwich-type panels. J Aeronaut Sci 1945;12(3):285–97.
[16] Hartness T, Husman G, Koening J, Dyksterhouse J. The characterization of low cost fiber reinforced thermoplastic composites produced by DRIFT process. Composites Part A 2001;32:1155–60.
[17] Company literature: Crane Composites, Inc. – a Crane Co. Company 23525 W Eames, Channahon, IL 60410, USA.
[18] Company literature: Universal Packaging, Inc., 2216 Greenspring Drive Lutherville, MD 21093.
[19] Morley M. Building with structural insulated panels. Newtown, CT: The Taunton Press; 2000.
[20] Annual book of ASTM standards C1583-04. Standard test method for tensile strength of concrete surfaces and the bond strength or tensile strength of concrete repair and overlay materials by direct tension (pull-off method). 100 Barr Harbor Drive, West Conshohocken, PA 19428-2959, United States; 2004.
[21] Operation manual, Dyna-Z-16. Proceq USA Inc., Aliquippa, PA 15001, USA.
[22] Annual book of ASTM standards E-72-05. Standard test method of conducting strength tests of panels for building construction. 100 Barr Harbor Drive, West Conshohocken, PA 19428-2959, United States; 2005.
[23] The Engineered Wood Association (APA). The engineered wood association product guide; 1998.
[24] Building code requirements for structural concrete (ACI 318-05) and commentary (ACI 318 R-05). American Concrete Institute.
[25] Vonach WK, Rammerstorfer FG. Wrinkling of thick orthotropic sandwich plates under general loading conditions. Arch Appl Mech 2000;70:338–48.
[26] Southward T, Mallinson GD, Jayaraman K, Horrigan D. Buckling of disbonds in honeycomb-core sandwich beams. J Sandwich Struct Mater 2008;10:195–216.
[27] Sleight DW, Wang JT. Buckling analysis of debonded sandwich panel under compression. NASA Tech, Memorandum 4701; 1995.
[28] Niu K, Talreja R. Buckling of a thin face layer on winkler foundation with debonds. J Sandwich Struct Mater 1999;1:259–78.
[29] Cox HL, Riddell JR. Sandwich construction and core materials III: instability of sandwich struts and beams. ARC technical report R&M 2125; 1945.
[30] Plantema FJ. Sandwich construction. New York: John Wiley and Sons; 1966.
[31] ANSYS manual. ANSYS 12.0A1 finite element analysis system. SAS IP, Inc.; 2010.
[32] Design guidelines of autoclaved aerated concrete panels. AERCON Florida LLC, Haines City, Florida. <http://www.aerconaac.com/index-4.html>.